Phase Behavior in Rhombohedral NaSiCON Electrolytes and Electrodes

—Supplementary Information—

Zeyu Deng,[*,†] Gopalakrishnan Sai Gautam,[‡] Sanjeev Krishna Kolli,[¶] Jean-Noël Chotard,[§,‖] Anthony K. Cheetham,[⊥,¶] Christian Masquelier,[§,‖] and Pieremanuele Canepa[*,⊥]

†*Department of Materials Science and Engineering, National University of Singapore, 9 Engineering Drive 1, 117575, Singapore*

‡*Department of Materials Engineering, Indian Institute of Science, Bangalore 560012, India*

¶*Materials Department and Materials Research Laboratory, University of California, Santa Barbara, California 93106, United States*

§*Laboratoire de Réactivité et Chimie des Solides, UMR CNRS #7314, Université de Picardie Jules Verne, 80039 Amiens Cedex, France*

‖*RS2E, Réseau Français sur le Stockage Electrochimique de l'Energie, FR CNRS #3459, F-80039 Amiens Cedex 1, France*

⊥*Department of Materials Science and Engineering, National University of Singapore, 9 Engineering Drive 1, Singapore*

E-mail: msedz@nus.edu.sg; pcanepa@nus.edu.sg

Contents

S1 Model Structure of $Na_{1+x}Zr_2Si_xP_{3-x}O_{12}$

Table S1 shows the atom labels and coordinates of the model-structure cell of $Na_{1+x}Zr_2Si_xP_{3-x}O_{12}$ on which the cluster expansion is fitted.

Table S1: Atom labels and fractional coordinates of the model-structure cell of $Na_{1+x}Zr_2Si_xP_{3-x}O_{12}$ in the rhombohedral representation. Space group $R\bar{3}c$ No. 167, lattice constants $a = 9.099$ Å and $\alpha = 60.634$ ° as obtained from Ref. 1, ICSD # 15546, with stoichiometry $Na_4Zr_2Si_3O_{12}$. The types of Na, i.e. Na(1) and Na(2) in reference to Figure 1 in the main article are also indicated.

Atomic species	**Label site**	**x**	**y**	**z**
Na/Va	0 Na(1)	0.500000	0.500000	0.500000
Na/Va	1 Na(1)	0.000000	0.000000	0.000000
Na/Va	2 Na(2)	0.889670	0.610330	0.250000
Na/Va	3 Na(2)	0.610330	0.250000	0.889670
Na/Va	4 Na(2)	0.250000	0.889670	0.610330
Na/Va	5 Na(2)	0.389670	0.750000	0.110330
Na/Va	6 Na(2)	0.750000	0.110330	0.389670
Na/Va	7 Na(2)	0.110330	0.389670	0.750000
Zr	8	0.352810	0.352810	0.352810
Zr	9	0.852810	0.852810	0.852810
Zr	10	0.647190	0.647190	0.647190
Zr	11	0.147190	0.147190	0.147190
Si/P	12	0.545440	0.954560	0.250000
Si/P	13	0.954560	0.250000	0.545440
Si/P	14	0.250000	0.545440	0.954560
Si/P	15	0.045440	0.750000	0.454560
Si/P	16	0.750000	0.454560	0.045440
Si/P	17	0.454560	0.045440	0.750000
O	18	0.432310	0.228140	0.579990
O	19	0.228140	0.579990	0.432310
O	20	0.579990	0.432310	0.228140
O	21	0.932310	0.079990	0.728140
O	22	0.079990	0.728140	0.932310
O	23	0.728140	0.932310	0.079990
O	24	0.567690	0.771860	0.420010
O	25	0.771860	0.420010	0.567690
O	26	0.420010	0.567690	0.771860
O	27	0.067690	0.920010	0.271860
O	28	0.920010	0.271860	0.067690
O	29	0.271860	0.067690	0.920010
O	30	0.469130	0.125870	0.329030
O	31	0.125870	0.329030	0.469130
O	32	0.329030	0.469130	0.125870
O	33	0.969130	0.829030	0.625870
O	34	0.829030	0.625870	0.969130
O	35	0.625870	0.969130	0.829030
O	36	0.530870	0.874130	0.670970
O	37	0.874130	0.670970	0.530870
O	38	0.670970	0.530870	0.874130
O	39	0.030870	0.170970	0.374130
O	40	0.170970	0.374130	0.030870
O	41	0.374130	0.030870	0.170970

S2 Analysis of the Effective Cluster Interactions

Table S2 and Figure S1 report the characteristics of the 65 distinct effective cluster interactions (ECIs) of the $Na_{1+x}Zr_2Si_xP_{3-x}O_{12}$ system in our cluster expansion (CE) model. Figure S1 plots the most significant ECIs (normalised by their multiplicity) as function of their index #.

Table S2: ECIs. Point term $\mathcal{PT}$, pair $\mathcal{P}$, triplet $\mathcal{T}$, and quadruplet $\mathcal{Q}$ terms. Site refer to the label sites given in Table S1. Cell $[0,0,0]$ is the reference cell. M is the multiplicity of each cluster.

Index	Cluster Index	Type	Site(Label)	Cell	Min. (Å)	Max. (Å)	ECI (meV)	ECI/M (meV)
1	4	$\mathcal{PT}$	Na/Va(3)	$[0,0,0]$	—	—	+54.194	+27.097
2	5	$\mathcal{P}$	Na/Va(3) Si/P(14)	$[0,0,0]$ $[0,0,0]$	3.055	3.055	–399.759	–33.313
3	6	$\mathcal{P}$	Na/Va(0) Na/Va(3)	$[0,0,0]$ $[0,0,0]$	3.162	3.162	–435.435	–72.572
4	8	$\mathcal{P}$	Na/Va(3) Si/P(17)	$[0,0,0]$ $[0,0,0]$	3.710	3.710	–570.255	–47.521
5	12	$\mathcal{P}$	Na/Va(3) Na/Va(6)	$[0,0,0]$ $[0,0,0]$	4.727	4.727	–42.419	–3.535
6	13	$\mathcal{P}$	Si/P(14) Si/P(15)	$[0,0,0]$ $[0,-1,1]$	4.922	4.922	+141.637	+11.803
7	14	$\mathcal{P}$	Na/Va(3) Na/Va(5)	$[0,0,0]$ $[0,1,-1]$	4.980	4.980	+58.296	+9.716
8	15	$\mathcal{P}$	Na/Va(3) Na/Va(4)	$[0,0,0]$ $[1,-1,0]$	5.102	5.102	+1193.520	+99.460
9	19	$\mathcal{P}$	Na/Va(3) Si/P(15)	$[0,0,1]$ $[1,-1,0]$	6.056	6.056	–385.829	–32.152
10	20	$\mathcal{P}$	Si/P(14) Na/Va(0)	$[0,0,0]$ $[0,0,1]$	6.173	6.173	+46.582	+3.882
11	21	$\mathcal{P}$	Na/Va(3) Si/P(14)	$[0,0,0]$ $[1,-1,0]$	6.196	6.196	–17.857	–1.488
12	22	$\mathcal{P}$	Na/Va(3) Si/P(17)	$[0,0,0]$ $[0,1,0]$	6.220	6.220	–352.738	–29.395
13	24	$\mathcal{P}$	Na/Va(3) Na/Va(0)	$[0,0,0]$ $[0,0,1]$	6.465	6.465	+468.440	+39.037
14	27	$\mathcal{P}$	Na/Va(3) Na/Va(0)	$[0,0,0]$ $[0,-1,1]$	6.519	6.519	+913.329	+76.111
15	30	$\mathcal{P}$	Na/Va(3) Si/P(15)	$[0,0,0]$ $[0,-1,1]$	6.901	6.901	+339.229	+28.269
16	31	$\mathcal{P}$	Na/Va(3)	$[0,0,0]$	6.956	6.956	+11.663	+1.944

			Na/Va(5)	$[0,0,0]$				
17	32	$\mathcal{P}$	Si/P(14) Si/P(15)	$[0,0,0]$ $[1,0,0]$	7.012	7.012	+3.121	+0.260
18	33	$\mathcal{P}$	Na/Va(3) Na/Va(7)	$[0,0,0]$ $[1,-1,0]$	7.263	7.263	–61.571	–5.131
19	34	$\mathcal{P}$	Na/Va(3) Na/Va(4)	$[0,0,0]$ $[0,-1,0]$	7.406	7.406	+670.671	+111.779
20	36	$\mathcal{P}$	Si/P(14) Si/P(16)	$[0,0,0]$ $[0,0,0]$	7.478	7.478	–145.242	–24.207
21	38	$\mathcal{P}$	Na/Va(3) Si/P(12)	$[0,0,0]$ $[0,-1,0]$	7.857	7.857	–445.839	–37.153
22	42	$\mathcal{P}$	Na/Va(3) Si/P(13)	$[0,0,0]$ $[-1,1,0]$	8.083	8.083	+276.618	+23.051
23	44	$\mathcal{P}$	Na/Va(3) Si/P(14)	$[0,0,0]$ $[0,-1,0]$	8.198	8.198	–377.133	–31.428
24	46	$\mathcal{P}$	Na/Va(3) Na/Va(5)	$[0,0,0]$ $[1,-1,0]$	8.483	8.483	+15.930	+2.655
25	49	$\mathcal{P}$	Si/P(14) Na/Va(0)	$[0,0,0]$ $[-1,1,0]$	8.570	8.570	–23.865	–1.989
26	50	$\mathcal{P}$	Si/P(14) Si/P(15)	$[0,0,0]$ $[1,-1,0]$	8.608	8.608	+130.803	+10.900
27	52	$\mathcal{P}$	Na/Va(3) Na/Va(7)	$[0,0,0]$ $[1,0,-1]$	8.736	8.736	–46.095	–3.841
28	53	$\mathcal{P}$	Na/Va(3) Na/Va(2)	$[0,0,0]$ $[0,-1,0]$	8.856	8.856	+11.860	+1.977
29	62	$\mathcal{P}$	Na/Va(3) Na/Va(3)	$[0,0,0]$ $[1,0,-1]$	9.186	9.186	–68.224	–11.371
30	63	$\mathcal{P}$	Na/Va(3) Na/Va(3)	$[0,0,0]$ $[1,0,-1]$	9.186	9.186	–142.789	–11.899
31	64	$\mathcal{P}$	Si/P(14) Si/P(14)	$[0,0,0]$ $[0,1,-1]$	9.186	9.186	-215.821	–17.985
33	65	$\mathcal{P}$	Na/Va(0) Na/Va(0)	$[0,0,0]$ $[1,0,-1]$	9.186	9.186	-561.834	–93.639
33	66	$\mathcal{P}$	Si/P(14) Si/P(14)	$[0,0,0]$ $[0,1,-1]$	9.186	9.186	–21.014	–3.502
34	69	$\mathcal{P}$	Na/Va(3) Si/P(14)	$[0,0,0]$ $[0,0,-1]$	9.309	9.309	+165.373	+13.781
35	71	$\mathcal{P}$	Si/P(14) Si/P(16)	$[0,0,0]$ $[-1,1,0]$	9.510	9.510	–142.597	–23.766
36	73	$\mathcal{P}$	Na/Va(3)	$[0,0,0]$	9.633	9.633	+21.698	+1.808

			Si/P(13)	$[0,-1,0]$				
37	79	$\mathcal{P}$	Na/Va(3) Si/P(17)	$[0,0,0]$ $[-1,0,1]$	9.838	9.838	+419.493	+34.958
38	82	$\mathcal{P}$	Na/Va(3) Si/P(12)	$[0,0,0]$ $[-1,-1,1]$	9.879	9.879	+183.989	+15.332
Index	**Cluster Index**	**Type**	**Site(Label)**	**Cell**	**Min. (Å)**	**Max. (Å)**	**ECI (meV)**	**ECI/M (meV)**
39	84	$\mathcal{T}$	Na/Va(3) Na/Va(0) Si/P(14)	$[0,0,0]$ $[0,0,0]$ $[0,0,0]$	3.056	3.739	–632.141	–52.678
40	85	$\mathcal{T}$	Na/Va(3) Na/Va(0) Si/P(13)	$[0,0,0]$ $[0,0,0]$ $[0,0,0]$	3.162	3.739	–343.491	–28.624
41	86	$\mathcal{T}$	Na/Va(3) Na/Va(0) Si/P(17)	$[0,0,0]$ $[0,0,0]$ $[0,0,0]$	3.478	3.739	+112.125	+9.344
42	87	$\mathcal{T}$	Na/Va(3) Si/P(14) Si/P(16)	$[0,0,0]$ $[0,0,0]$ $[0,0,1]$	3.056	4.626	–8.603	-0.717
43	88	$\mathcal{T}$	Na/Va(3) Si/P(14) Si/P(12)	$[0,0,0]$ $[0,0,0]$ $[0,-1,1]$	3.056	4.700	+147.373	+24.562
44	89	$\mathcal{T}$	Si/P(14) Si/P(12) Si/P(13)	$[0,0,0]$ $[0,-1,1]$ $[-1,0,1]$	4.700	4.700	+36.538	+18.269
45	91	$\mathcal{T}$	Na/Va(3) Na/Va(6) Si/P(13)	$[0,0,0]$ $[0,0,0]$ $[0,0,0]$	3.162	4.727	+210.952	+17.579
46	92	$\mathcal{T}$	Na/Va(3) Na/Va(0) Na/Va(6)	$[0,0,0]$ $[0,0,0]$ $[0,0,0]$	3.477	4.727	+2969.345	+247.445
47	93	$\mathcal{T}$	Na/Va(3) Si/P(14) Si/P(17)	$[0,0,0]$ $[0,0,0]$ $[0,0,0]$	3.056	4.922	+124.056	+10.338
48	96	$\mathcal{T}$	Si/P(14) Si/P(15) Si/P(16)	$[0,0,0]$ $[0,0,0]$ $[-1,0,1]$	4.626	4.922	+101.874	+8.490
49	98	$\mathcal{T}$	Na/Va(3) Na/Va(4) Si/P(13)	$[0,0,0]$ $[1,-1,0]$ $[0,0,0]$	3.055	5.102	–167.327	-13.944
50	99	$\mathcal{T}$	Na/Va(3)	$[0,0,0]$	3.4779	5.102	-483.709	–40.309

			Na/Va(4) Na/Va(1)	$[1,-1,0]$ $[1,0,1]$				
51	100	$\mathcal{T}$	Na/Va(3) Na/Va(4) Na/Va(7)	$[0,0,0]$ $[1,-1,0]$ $[1,0,0]$	4.727	5.102	+85.713	+7.143
52	101	$\mathcal{T}$	Na/Va(0) Na/Va(4) Na/Va(6)	$[0,0,0]$ $[1,-1,0]$ $[0,0,0]$	4.727	5.102	–193.556	–16.130
53	102	$\mathcal{T}$	Na/Va(3) Na/Va(4) Na/Va(2)	$[0,0,0]$ $[1,-1,0]$ $[0,-1,1]$	5.1025	5.1025	–96.748	–24.187
54	104	$\mathcal{T}$	Si/P(14) Na/Va(0) Si/P(12)	$[0,0,0]$ $[0,0,0]$ $[0,0,0]$	3.739	5.629	+913.076	+76.090
55	105	$\mathcal{T}$	Si/P(14) Si/P(12) Si/P(17)	$[0,0,0]$ $[0,0,0]$ $[0,0,0]$	4.626	5.629	+183.298	+15.275
56	107	$\mathcal{T}$	Si/P(14) Si/P(12) Si/P(15)	$[0,0,0]$ $[0,0,0]$ $[0,0,0]$	4.922	5.629	–64.742	–5.395
57	108	$\mathcal{T}$	Si/P(14) Si/P(12) Si/P(13)	$[0,0,0]$ $[0,0,0]$ $[0,0,0]$	5.623	5.623	–110.756	–27.689
58	109	$\mathcal{T}$	Na/Va(3) Si/P(14) Na/Va(2)	$[0,0,0]$ $[0,0,0]$ $[-1,0,1]$	3.056	5.733	–15.573	–2.595
59	110	$\mathcal{T}$	Na/Va(3) Na/Va(6) Na/Va(5)	$[0,0,0]$ $[0,0,0]$ $[0,-1,1]$	4.727	5.733	–237.045	–19.754
60	111	$\mathcal{T}$	Na/Va(3) Na/Va(4) Na/Va(2)	$[0,0,0]$ $[1,-1,0]$ $[0,0,0]$	5.103	5.733	–54.373	–9.062
61	112	$\mathcal{T}$	Na/Va(3) Na/Va(4) Na/Va(2)	$[0,0,0]$ $[0,-1,1]$ $[-1,0,1]$	5.733	5.733	–32.485	–16.243
Index	**Cluster Index**	**Type**	**Site(Label)**	**Cell**	**Min. (Å)**	**Max. (Å)**	**ECI (meV)**	**ECI/M (meV)**
62	113	$\mathcal{Q}$	Na/Va(3) Na/Va(0) Na/Va(6) Si/P(17)	$[0,0,0]$ $[0,0,0]$ $[0,0,0]$ $[0,0,0]$	3.162	4.727	–648.492	–54.041

63	115	$\mathcal{Q}$	Na/Va(3) Na/Va(6) Si/P(13) Si/P(17)	[0, 0, 0] [0, 0, 0] [0, 0, 0] [0, 0, 0]	3.056	4.922	–125.232	–10.436
64	118	$\mathcal{Q}$	Na/Va(3) Na/Va(0) Si/P(13) Si/P(17)	[0, 0, 0] [0, 0, 0] [0, 0, 0] [0, 0, 0]	3.162	4.922	–748.192	–62.349
65	119	$\mathcal{Q}$	Na/Va(3) Si/P(14) Na/Va(5) Si/P(16)	[0, 0, 0] [0, 0, 0] [0, 0, 1] [0, 0, 1]	3.056	4.981	–55.110	–9.185

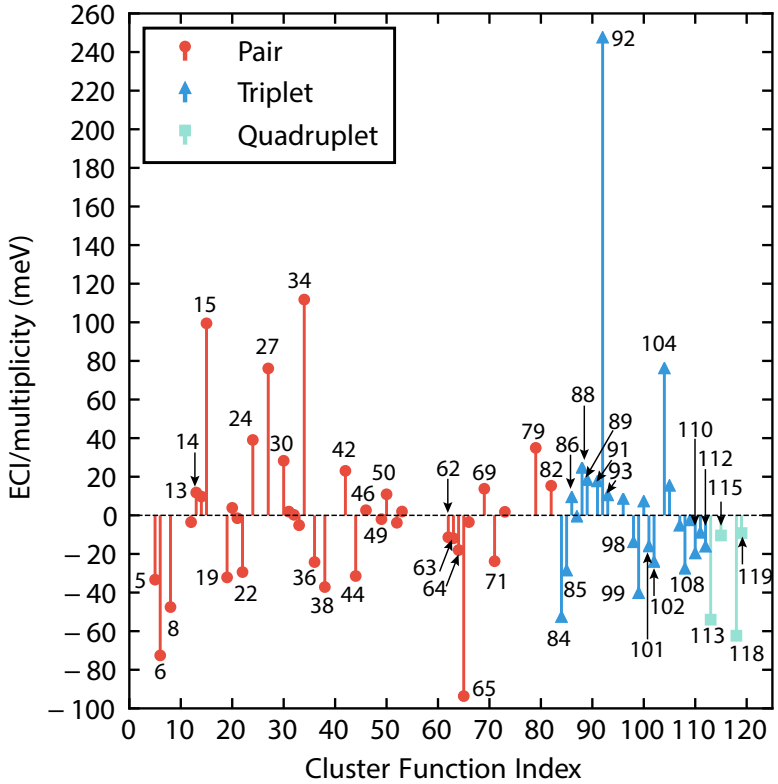

Figure S1: Relevant ECIs as function vs. their cluster index as fully detailed in Table S2. The point term is not shown.

S3 Basis of the Cluster Expansion and ECI assignation

An occupational basis was utilised and thus σ is assigned Na = 0, Va = 1, and Si = 0, P = 1. Therefore only clusters which are occupied by Va (on Na/Va sites) and/or P (on Si/P sites) in a given structure contribute non-zero ECIs to the overall CE model. The sign of the ECIs identify whether the interactions are attractive (negative ECIs) or repulsive (positive ECIs) between Va, P and across Va and P. While an attractive ECI favors all sites in a given cluster to be occupied by Va and/or by P, a repulsive ECI favors the occupation of at least one of the sites in the cluster by Na or Si. Tables S3, S4, and S5 lists the most prominent, in terms of magnitude, attractive and repulsive pair, triplet, and quadruplet ECIs, respectively.

Table S3: Unique ECI pairs (in meV) normalised by their multiplicity.

ECI #	**Species**	**ECI**
	Attractive	
5	Va–P	–33.313
6	Va–Va	–72.572
8	Va–P	–47.521
19	Va–P	–32.152
22	Va–P	–29.395
36	P–P	–24.207
38	Va–P	–37.153
44	Va–P	–31.428
64	P–P	–17.985
65	Va–Va	–93.639
71	Va–P	–23.766
	Repulsive	
15	Va–Va	+99.460
24	Va–Va	+39.037
27	Va–Va	+76.111
30	Va–P	+28.269
34	Va–Va	+111.779
42	Va–P	+23.051
79	Va–P	+34.958

Table S4: Unique ECI triplets (in meV) normalised by their multiplicity.

ECI #	Species	ECI
	Attractive	
84	Va–Va–P	–52.678
85	Va–Va–P	–28.624
99	Va–Va–Va	–40.309
102	Va–Va–Va	–24.187
	Repulsive	
92	Va–Va–Va	+247.445
104	P–Va–P	+76.090

Table S5: Unique ECI quadruplets (in meV) normalised by their multiplicity.

ECI #	Species	ECI/M (meV)
	Attractive	
113	Va–Va–Va–P	–54.041
118	Va–Va–P–P	–62.349

S4 Thermodynamic Integration

As shown in Figure S2, the grand-canonical Monte Carlo (MC) scans were performed in the chemical potential (μ) and temperature (T) space. The scan started at $T = 5$ K and up to 1605 K with a step $\Delta T = 5$ K at $\mu = -1$, 0 and 1 eV/f.u. Then at every T, μ was scanned in both forward ($\mu = -1.0$ to 1.0 eV/f.u.) and backward ($\mu = 1.0$ to –1.0 eV/f.u.) directions with a step size of $\Delta\mu = 0.005$ eV/f.u. as shown in Figure S2. In general, μ was scanned across 2 concentration ranges, namely, between x = 0 and 2 ($\mu = -1.0$ to 0.0 eV/f.u.), and x = 2 and 3 ($\mu = 0.0$ to 1.0 eV/f.u.), due to the existence of the 3 ground-state structures on the convex hull (x = 0, 2 and 3, see manuscript).

The phase boundary was found at the intersections of the grand-canonical potential energy Φ^α for each phase α (A, B and C) as defined in Figure S2. Φ is defined by Eq. 1

$$\Phi = [E - \mathrm{T}S] - \mu c \tag{1}$$

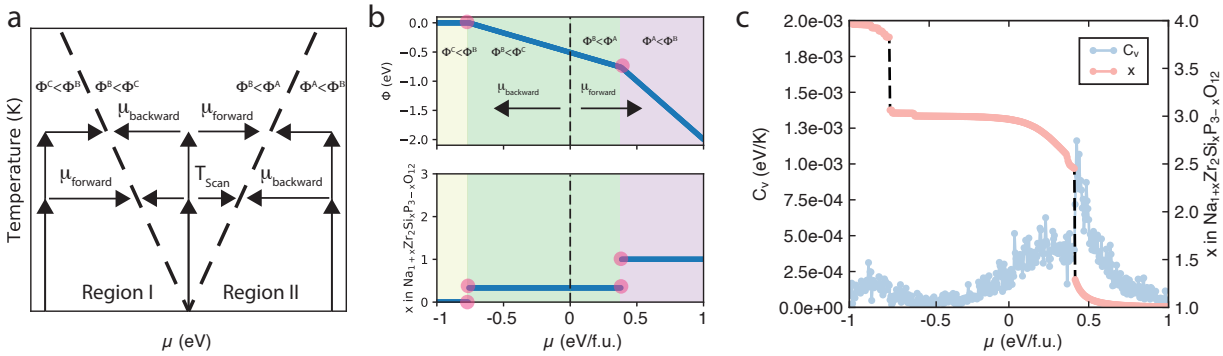

In panel

Figure S2: **a** Schematic showing how the phase boundary (dashed lines) was identified in the (μ, T) space. The arrows show both the MC scan and the thermodynamic integration directions. At phase boundaries, potential surfaces $\Phi^{\alpha}(\mu, T)$ on the both sides intersects with each other. The phase boundaries in the (x, T) space are then converted from the compositions at the phase boundary in (μ, T) space. **b** An example (at T = 105 K) of the grand potential (Φ) depending on chemical potential (μ, T), along with the strategy to choose the phase boundaries (pink circles) is shown. **c** Variation of composition x and normalized heat capacity C_v vs. μ, at T = 445 K, as obtained from the Monte Carlo simulations is displayed. Discontinuities in the chemical potential μ represent phase transitions at specific concentrations x and are indicated by dashed lines in black.

where E is the total energy predicted by the cluster expansion model, S is the configurational entropy and c is the parametric composition. The parametric composition c in $Na_{1+x}Zr_2Si_xP_{3-x}O_{12}$ is defined as in Eq. 2.

$$c = 1 - \frac{x}{3} \quad \text{with} \quad 0 \leq c \leq 1. \tag{2}$$

For Monte Carlo scans at fixed μ and variable T, Φ is calculated using the thermodynamic integration in Eq. 3.

$$\Phi(\beta, \mu) = \frac{\beta_0}{\beta}\Phi_0(\beta_0, \mu) + \frac{1}{\beta}\int_{\beta_0}^{\beta} [E - \mu c]\, d\beta \tag{3}$$

$$\text{with} \quad \Phi_0(\beta_0, \mu) = E - \mu c \tag{4}$$

where $\beta = 1/(k_B T)$ and k_B is the Boltzmann constant.

In Monte Carlo scans at variable μ and fixed T, Φ is defined in Eq. 5.

$$\Phi(\beta,\mu) = \Phi_0(\beta,\mu_0) - \frac{1}{\beta}\int_{\mu_0}^{\mu} c d\mu \quad (5)$$

$$\text{with } \Phi_0(\beta,\mu_0) = \Phi_{\text{heating}}(\beta,\mu_0) \quad (6)$$

Since the entropy effects are negligible at low temperatures (e.g., $T = 5$ K), the starting values of Φ_0 in T scans at 5 K are taken as $\Phi_0 = E - \mu c$. The thermodynamic integration at each μ starts from the $\Phi_{heating}(T,\mu_0)$ where μ_0 = -1, 0 and 1 eV/f.u., and is scanned both forward and backward in the Region I and Region II as shown in Figure S2**a**. One of the examples is shown in Figure S2**b**.

After the thermodynamic integration, the phase boundary is identified by the intersection of grand-canonical potential envelops in the (μ, T) space (dashed lines in Figure S2**a**) which is then converted into the (x, T) space. When the intersections is not well defined by the numerical data, discontinuities in c vs. μ and C_v vs. μ curves (see Figure S2**c**) are considered and the phase boundaries identified.

S5 Monte Carlo Snapshot and Ground States Structures

Figure S3 shows a snapshot from the Monte Carlo simulations and three ground state structures at x = 0, 2 and 3 in $Na_{1+x}Zr_2Si_xP_{3-x}O_{12}$ (right panel).

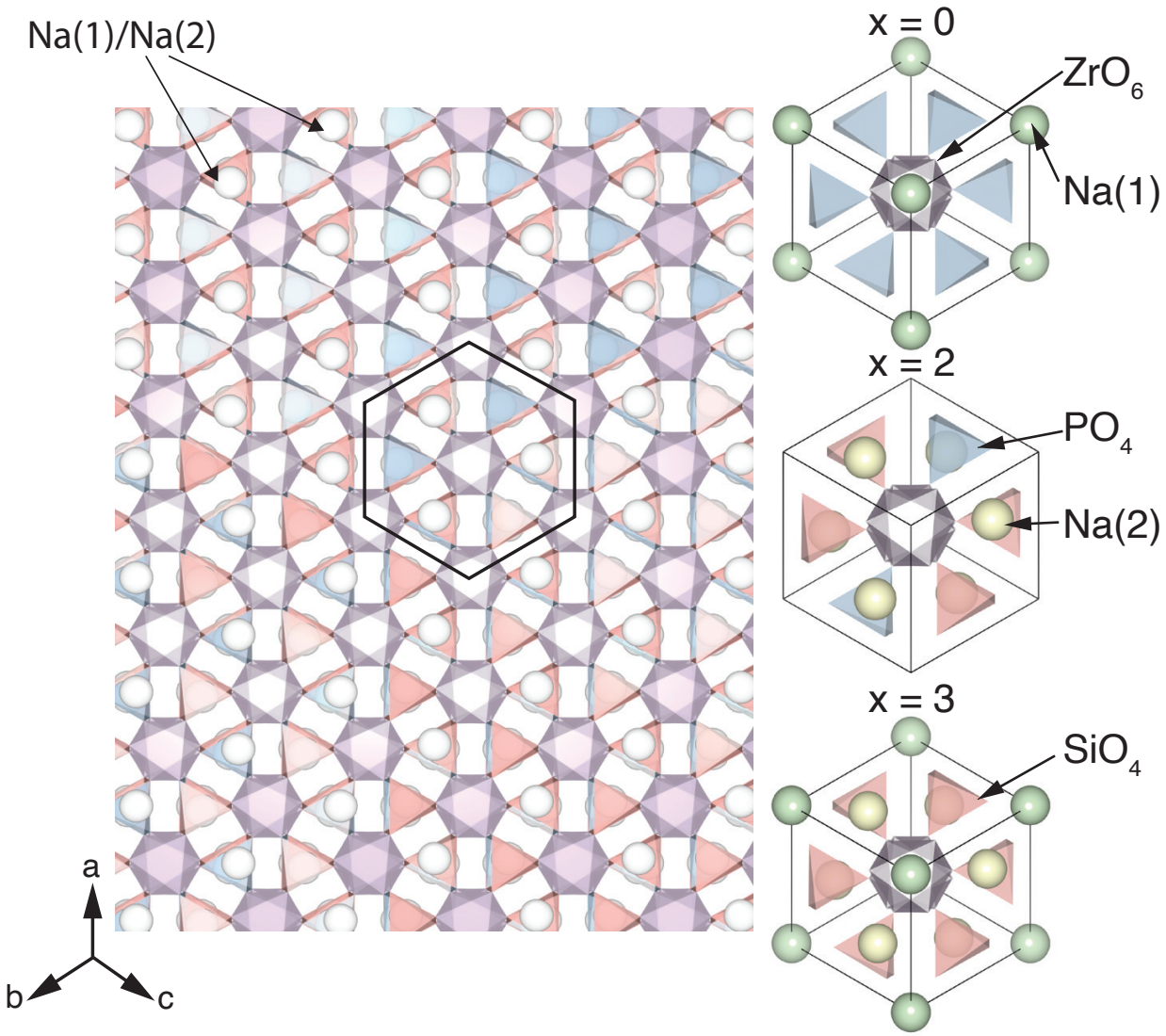

Figure S3: In the left panel, a portion of a snapshot of a Monte Carlo simulation (x = 2, T = 445 K), where a primitive cell of $Na_{1+x}Zr_2Si_xP_{3-x}O_{12}$ is marked by the black hexagon (Na at both Na(1) and Na(2) sites are coloured silver). The primitive cells of the three ground state structures at x = 0, 2 and 3 for $Na_{1+x}Zr_2Si_xP_{3-x}O_{12}$ are shown on the right.

Figure S4 displays another view of the three ground-state orderings as isolated from our

DFT calculations.

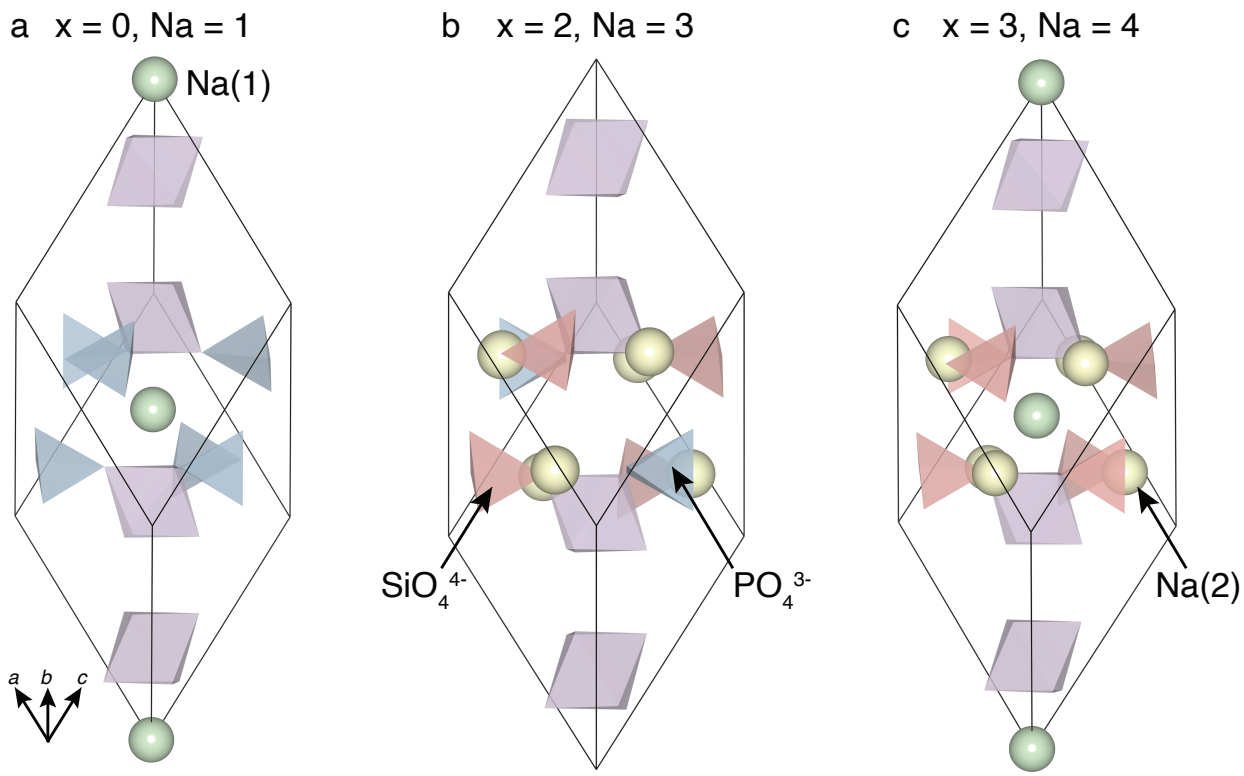

Figure S4: Ground-state structures in the rhombohedral setting identified in the convex hull of Figure 2 of the main manuscript. Panel **a**, the ground-state structure at Na = 1 (x = 0), **b** ground-state structure at Na = 3 (x = 2), and **c** ground-state structure at Na = 4 (x = 3) in $Na_{1+x}Zr_2Si_xP_{3\text{-}x}O_{12}$. The different sodium sites Na(1) and Na(2) are identified by green and yellow balls. SiO_4^{4-} and PO_4^{3-} tetrahedra are shown in pink and blue, respectively.

At Na = 1 (x = 0) (Figure S4**a**) only the Na(1) sites are occupied, whereas Na = 3 (x = 2) only the Na(2) sites are occupied (panel **b**). In Figure S4**c**, which is a representation of Na = 4 (x = 3), both Na(1) and Na(2) sites are occupied. Notably, at both Na = 1 (x = 0) and Na = 4 (x = 3) the $Na_{1+x}Zr_2Si_xP_{3\text{-}x}O_{12}$ structure arranges into a rhombohedral symmetry $R\bar{3}c$ (167), whereas Si/P and Na ions Na = 3 (x = 2) are organised in the $C2/c$ (15) space group.

S6 P^{5+} Migration Barrier in $Na_{1+x}Zr_2Si_xP_{3-x}O_{12}$

Figure S5 shows the migration barrier of a P^{5+} ion in $Na_{1+x}Zr_2Si_xP_{3-x}O_{12}$ via a vacancy mechanism. The migration barrier was computed using the nudged elastic band method[2] and the DFT settings employed in the manuscript. To facilitate the convergence of this barrier we used Perdew, Burke, and Ernzerhof[3] exchange and correlation functional. A large 2×1×1 supercell of the conventional cell (with 288 atoms) was used to minimised the spurious interaction between adjacent migration paths. The total energy was converged to 1×10^{-5} eV and the forces on the elastic band to 100 meV/Å.

Unsurprisingly, the displacement of a P^{5+} ions from the PO_4^{3-} moieties is extremely energy intensive (with a barrier of $\sim$ 4.02 eV, Figure S5), and suggests that the redistribution of P and Si in $Na_{1+x}Zr_2Si_xP_{3-x}O_{12}$ is highly inhibited even under high temperatures.

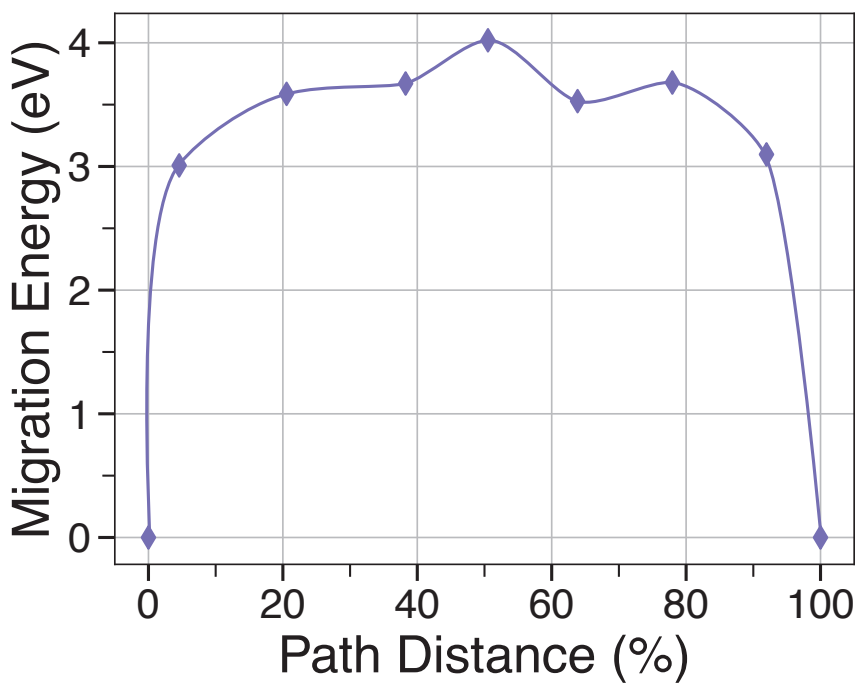

Figure S5: Migration barrier (in eV) of P^{5+} in the $Na_{1+x}Zr_2Si_xP_{3-x}O_{12}$ structure vs. the path distance.

References

(1) Qui, D.; Capponi, J.; Joubert, J.; Shannon, R. Crystal structure and ionic conductivity in $Na_4Zr_2Si_3O_{12}$. *J. Solid State Chem.* **1981**, *39*, 219–229.

(2) Sheppard, D.; Terrell, R.; Henkelman, G. Optimization methods for finding minimum energy paths. *J. Chem. Phys.* **2008**, *128*, 134106.

(3) Perdew, J. P.; Burke, K.; Ernzerhof, M. Generalized Gradient Approximation Made Simple. *Phys. Rev. Lett.* **1996**, *77*, 3865–3868.